AUTONOMOUS DRIVING CONTROL OF A ROBOTIC MOWER ON SLOPES USING A LOW-COST TWO-FREQUENCY GNSS COMPASS AND AN IMU

Sho Igarashi[1], Yutaka Kaizu[1,*], Toshio Tsutsumi[2], Kenichi Furuhashi[1], Kenji Imou[1]

[1] Graduate School of Agricultural and Life Sciences, The University of Tokyo, Bunkyo-ku, Japan.
[2] Sanyokiki Co. Ltd., Asaguchi, Okayama, Japan.
[*] Correspondence: kaizu@g.ecc.u-tokyo.ac.jp, yuta_kaizu@yahoo.co.jp

HIGHLIGHTS

- In this study, we developed an autonomous driving system for a robotic mower operating on a slope.
- RTK-GNSS, a GNSS compass, and an IMU were used as sensors for the robotic mower.
- Autonomous driving tests on a slope showed that the driving accuracy of the system was sufficient to meet the requirements of mowing work.

ABSTRACT. *An autonomous driving control system for a robotic mower was designed using a low-cost dual-frequency global navigation satellite system (GNSS) compass, a low-cost dual-frequency real-time kinematic GNSS (RTK-GNSS), and an inertial measurement unit (IMU). The intended application is to save labor by autonomously mowing sloped terrains. To investigate the effectiveness of the prototype GNSS compass on an inclined terrain, the roll, pitch, and yaw angles were varied using an inclined stage, and the heading accuracy was evaluated. The root mean square (RMS) of the heading error was within 1.5° when the roll and pitch angles were both less than 45°. Autonomous driving tests were conducted on the slope of an agricultural dam with an incline of approximately 25°. The prototype GNSS compass was capable of continuous and consistent heading measurements even on the slope. The cross-track error for the set path was 7.2 cm RMS when starting near the top and driving down the slope. When the robot started near the bottom of the slope and ran up, the cross-track error was 6.6 cm RMS. For the mower and experimental conditions used in this study, this was sufficient accuracy for autonomous driving when mowing on a slope.*

Keywords. *Heading angle, Inclination, MAVLink, Moving baseline, Robot operation system (ROS).*

In recent years, automatic steering of agricultural machines such as tractors, combine harvesters, and rice transplanters has been realized to improve the efficiency of farm work (Roshanianfard et al., 2020; Rains et al., 2014). These machines often incorporate an automatic control system consisting of a global navigation satellite system (GNSS) receiver that can determine the position of the vehicle and an inertia measurement unit (IMU) that can measure its heading and attitude. This system allows the machine to run automatically along a predetermined path (Carballido et al., 2014; Bochtis et al., 2009). For the vehicle position, the use of real-time kinematic (RTK)-GNSS enables positioning with an error of a few centimeters. Vehicle orientation is estimated by sensor fusion, i.e., the combination of sensors, such as accelerometers, gyroscopes, and magnetometers, and GNSS (Mousazadeh, 2013; Lindgren et al., 2002). A single sensor may not provide the correct heading of a moving vehicle due to measurement errors. If there is a measurement error in the gyroscope sensor that measures the angular velocity, then the heading angle, which is the integrated value of the angular velocity, gradually shifts as errors accumulate. Due to the low signal-to-noise (SN) ratio of the magnetic field to be measured, it is difficult to accurately measure the orientation using only a magnetometer. Although GNSS can measure the direction of antenna movement by Doppler shift and the movement vector between measurement epochs, the measured result for the direction of movement is not always the same as the actual heading of the vehicle. The yaw angle is also susceptible to magnetic disturbance even when sensor fusion is performed by filtering the measured values of these sensors (Shen et al., 2021). Such disturbances are likely to occur when the machine is moved to a different test site or the equipment configuration is changed, and the solution requires an onerous calibration procedure. For accurate calibration, it is necessary for the machine to be rotated in all directions with the sensor system attached to ensure the ability to accurately measure roll,

Submitted for review on 22 January 2022 as manuscript number ITSC 15032; approved for publication as a Research Article by Associate Editor Dr. Joe Dvorak and Community Editor Dr. Naiqian Zhang of the Information Technology, Sensors, & Control Systems Community of ASABE on 16 June 2022.

pitch, and yaw (Qureshi and Golnaraghi, 2017). For lightweight machines such as small unmanned aerial vehicles (UAVs), calibration is relatively easy, but larger and heavier machines such as agricultural machinery can only be rotated horizontally. In addition, the horizontal vector of the geomagnetic field varies from place to place on Earth, so it is necessary to compensate for declination.

However, a sensor system using multiple GNSS receivers (hereinafter referred to as a GNSS compass) is a method of measuring heading with several advantages: it does not require calibration, it can measure absolute heading even when stationary, and it does not need to consider declination. As shown in figure 1a, two antennas are installed on a moving vehicle: one antenna is the reference station, and the other antenna is the rover station with a certain spacing between the two antennas. The absolute heading angle θ can be obtained by measuring the vector between the antennas using the RTK principle, which is called moving-base RTK. Some commercial GNSS compasses incorporate two antennas and receivers in a single housing, while others have external antennas and allow the distance between the antennas to be freely changed. The method of using multiple GNSS receivers to measure the position and heading of a vehicle has been applied to mobile robots such as a robotic boat to take measurements in a lake environment (Kaizu et al., 2015), a robotic combine harvester (Mochizuki et al., 2015; Iida et al., 2013) and a tractor (Bell, 2000). As shown in figure 1b, the heading can be measured by determining the positions of the antennas of the two mobile stations on the vehicle relative to the stationary reference station. Wang et al. (2016) used two RTK-GNSS receivers to measure the heading of a ground vehicle for high-throughput plant phenotyping. Kaizu et al. (2018) used two low-cost RTK-GNSS receivers to measure the heading of a robotic mower to evaluate the accuracy of driving control.

In the past, RTK-GNSS receivers were expensive, so the use of multiple receivers for orientation measurement was limited to cases where the machine itself was expensive, such as the blade control of a bulldozer. In recent years, low-cost RTK-GNSS receivers have become available. Therefore, it has become possible to add autonomous driving functions using a GNSS compass to small and inexpensive machines, such as robotic mowers (Igarashi et al., 2020). In their study, a low-cost single-frequency RTK-GNSS receiver was used. Today, higher performance and inexpensive dual-frequency RTK-GNSS receivers are readily available. Dual-frequency RTK-GNSS receivers are advantageous in practice because they take less time than single-frequency receivers to converge RTK positioning. However, conventional dual-frequency RTK-GNSS receivers for land surveying cost more than \$10,000. In recent years, lower-cost dual-frequency RTK-GNSS receivers have become available, and their evaluation boards are very inexpensive (approximately \$249). Therefore, it is more economical to use even two receivers than a high-precision gyroscope sensor or a magnetometer sensor with guaranteed accuracy and benefit from the advantages of the GNSS compass described above.

Farming operations such as plowing, hauling, and mowing often involve working on slopes and uneven terrain. To save labor, it is necessary to drive agricultural machines on slopes and uneven terrain, and several attempts have been made thus far to develop autonomous driving controls for these agricultural machines. Mashadi and Nasrolahi (2009) designed a control system for a tractor moving on a slope to prevent accidental falls from agricultural machines. Tamaki et al. (2006) tested automatic straight-line driving of a crawler vehicle on a grassland with an inclination angle of 11°. By using two Doppler velocity sensors, the velocity difference between the front and rear of the vehicle caused by the pitch angle was averaged to improve the position estimation accuracy. However, no studies of an autonomous robotic mower driving on a slope using multiple GNSS receivers have been published. In mowing work, it is necessary to operate the mower not only on flat areas but also on slopes of 30° to 40°. On a slope, the accuracy of the heading measurement may be degraded due to the decrease in the received signal level caused by the tilting of the antenna and the blocking of the satellite signal in the upslope direction. Therefore, it is very important to investigate whether positioning and orientation measurements can be performed even when the antenna is inclined.

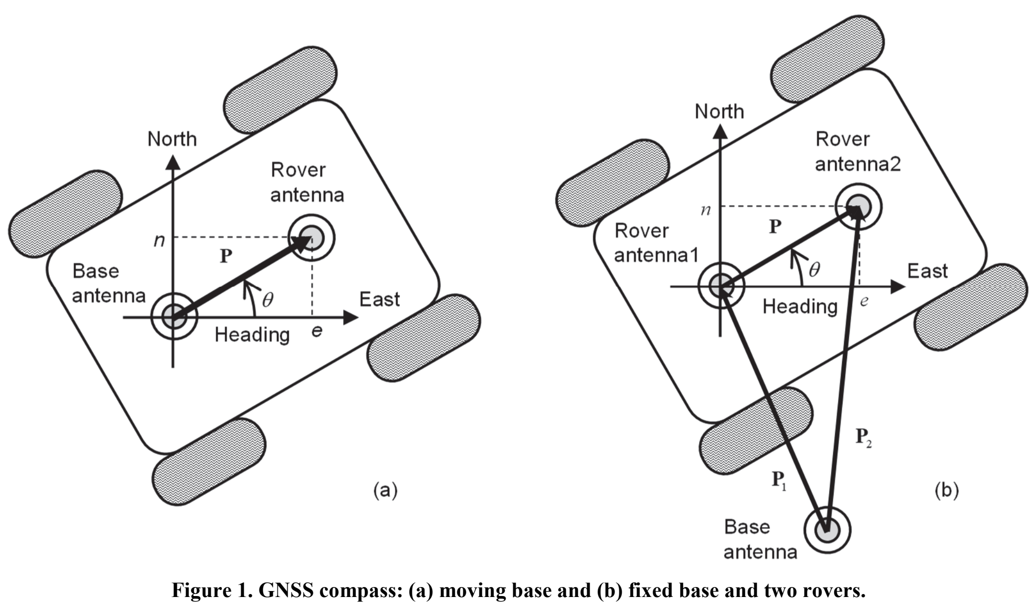

Figure 1. GNSS compass: (a) moving base and (b) fixed base and two rovers.

In this study, we constructed a GNSS compass system using two low-cost dual-frequency RTK-GNSS receivers, investigated its orientational measurement accuracy, and evaluated the effect of antenna tilt on the orientational measurement accuracy. In addition, the GNSS compass was mounted on a robotic mower and tested for autonomous driving on a slope with an angle of approximately 25°. These tests were used to evaluate the effectiveness of this system while mowing on sloping ground.

Materials and Methods

Accuracy Evaluation of a Low-cost Dual-frequency GNSS Compass

Overview of the Accuracy Evaluation Device and System

Figure 2 shows the system used to experimentally evaluate the prototype GNSS compass. Two dual-frequency multi-GNSS antennas were mounted 50 cm apart on an aluminum tube with a square cross-section (hereinafter referred to as an antenna set).

A motorized rotation stage (ARS-436HM, Chuo Precision Industrial Co., Ltd., Tokyo, Japan) for roll rotation, a manual tilt stage (TS-211, Chuo Precision Industrial Co., Ltd., Tokyo, Japan) for pitch rotation, and a motorized rotation stage (MM-60θ, Chuo Precision Industrial Co., Ltd., Tokyo, Japan) for yaw rotation were fixed on a tripod. The antenna set was installed on the top stage. The motorized stages were driven by stepping motors with a resolution of 0.01° for roll rotation and 0.008° for yaw rotation, and the positioning accuracies were 0.18° and 0.15°, respectively. The antenna set can be placed in any posture in the range of ±60° for roll rotation, from 0 to 60° for pitch rotation, and from 0 to 360° for yaw rotation. Figure 2b shows the case when the roll and pitch rotation angles were each set to 60°.

The block diagram of the evaluation system is shown in figure 3. The GNSS signals received by antenna 1 and antenna 2 were divided by signal splitters and fed to a commercial GPS (global positioning system) compass (VS-101, Hemisphere Inc., Scottsdale, Ariz.) and a prototype GNSS compass consisting of two low-cost dual-frequency RTK-GNSS receivers (C099-F9P-0, u-blox AK, Thalwil, Switzerland). Patch antennas (ANN-MB-00, u-blox AK, Thalwil, Switzerland) were used as the GNSS antennas.

The commercial GPS compass was used as a basis for accuracy comparison with the low-cost dual-frequency RTK-GNSS compass proposed in this study. The commercial GPS compass was a single-frequency receiver that used only GPS for the positioning satellite. It measured the heading using a moving-base RTK with the coarse/acquisition (C/A) code of the L1 signal and the phase information of the L1 carrier. According to catalog values, the heading accuracy was less than 0.3° root mean square (RMS) when using the supplied antennas with a baseline length of 0.5 m (Hemisphere Inc, 2010). In terms of the RTK positioning performance of the receiver used for the prototype GNSS compass, the convergence time of RTK positioning was within 10 seconds when the baseline length was 1 km. The horizontal accuracy was 0.01 m + 1 ppm × baseline length (within 20 km) circular error probability (CEP, mean error radius) (u-blox AG, 2020). The prototype GNSS compass used the moving-base RTK function of the receivers to measure the heading; however, the heading measurement accuracy was not described in the data sheet.

The position and heading measurement results from the commercial GPS compass and the prototype GNSS compass were recorded on a laptop PC using a universal serial bus (USB). The obtained messages were HDT (heading) and National Marine Electronics Association (NMEA)-GGA for the commercial GPS compass and UBX-NAV-RELPOSNED for the prototype GNSS compass. UBX-NAV-RELPOSNED is a proprietary format of u-blox receivers that includes the position of the mobile station antenna relative to the reference station antenna in millimeters.

Experimental Conditions and Orientational Measurement Method

The experiment was conducted on a rooftop at the building of the University of Tokyo in Bunkyo-ku, Tokyo, Japan (latitude: 35.716751° N, longitude: 139.759975° E) where

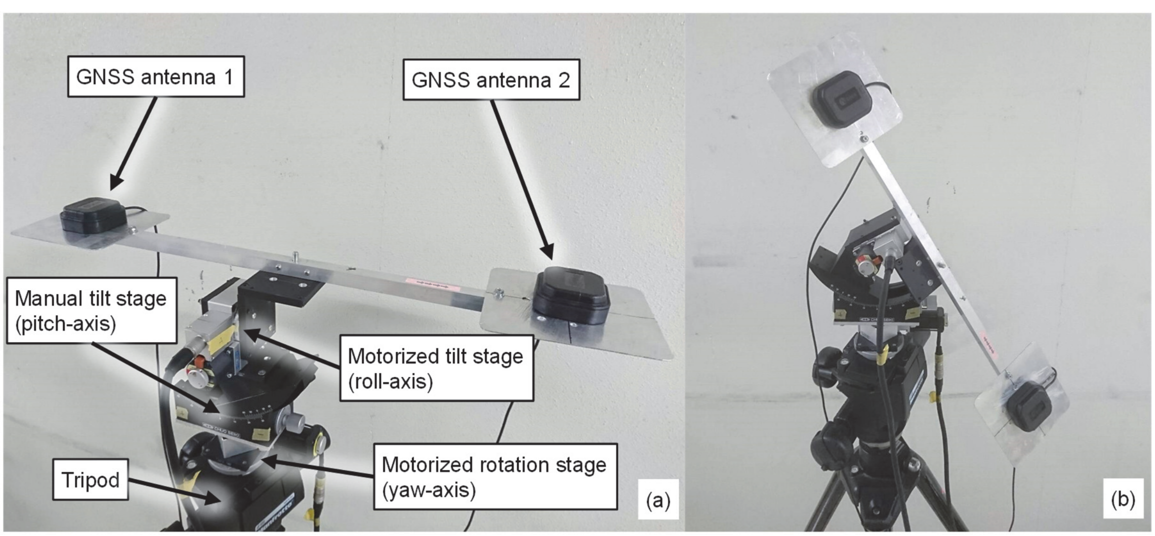

Figure 2. Device used for evaluation of dual-frequency RTK-GNSS compass: (a) horizontal state and (b) state of maximum angle of inclination (roll angle 60°, pitch angle 60°).

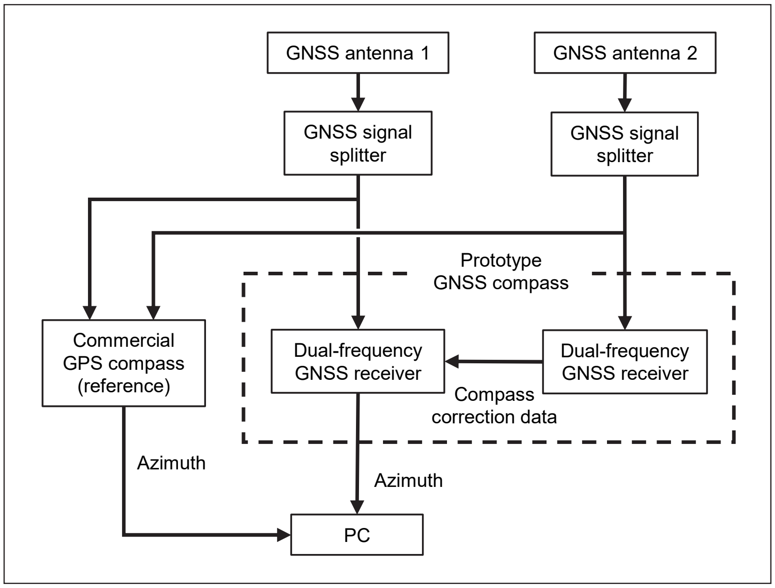

Figure 3. Schematic diagram of evaluation system for a low-cost RTK-GNSS compass.

the sky was not obstructed by other buildings. The tripod was adjusted with the antenna at a height of 1.6 m above the floor.

To evaluate the effect of the angle change on the heading accuracy, the roll, pitch, and yaw angles were varied, and the azimuth angle was measured by the accuracy evaluation system described above. First, the roll and pitch angles of the antenna set were both set to 0°. The yaw angle was rotated by 45° every 10 seconds by the motorized rotation stage. After the yaw angle was rotated from 0° to 315°, it was returned to 0°. Then, the roll angle was changed by the motorized rotation stage, and the yaw angle was automatically rotated as previously described. When the yaw angle reached 315° again, it was returned to 0°, and the roll angle was varied again. This operation was repeated nine times with the roll angle from -60° to 60° and an angle change range of 15°. All of the above changes in yaw angle and roll angle were performed automatically by a program. After the above operations were completed, the pitch angle was changed by 15° using a manual rotation stage, and the same operations as above were performed for the roll angle and yaw angle. The pitch angle was varied to five values: 0°, 15°, 30°, 45°, and 60°. To exclude the time of the stage rotation (approximately 2 seconds), the measured heading angles, from three seconds after the start of rotation to ten seconds during the stage was stationary, were averaged and analyzed.

True Heading Estimation and Evaluation Methods

The purpose of this study is to evaluate the error of the prototype GNSS compass with respect to the true heading. To accurately determine the true heading, the following method was used to calculate the offset between the set angle of yaw indicated by the rotary table and the true heading. Generally, an astronomical observation, a gyrotheodolite, or a survey of known points is used to determine the true heading. Since these methods were not available in this experiment, we used a commercial GPS compass as a more convenient alternative. Once the offset was determined, the angle of the rotation stage was converted to the true heading.

Assuming that the commercial GPS compass had less error than the prototype GNSS compass and that the average error for each direction became zero, the antenna set was rotated by 45° from 0° to 315° with the yaw setting angle in 45° increments, while the antenna set was horizontal with both roll and pitch angles of 0°. At each yaw angle, we calculated the average heading of the commercial GPS compass measurements of 8 seconds. The difference between the average heading angle and the yaw setting angle was averaged to obtain the offset angle. If the difference was negative, then 360° was added. The sum of the yaw set angle and the offset angle was considered the true heading.

Then, we evaluated the accuracy of the heading by comparing the heading output from the prototype GNSS compass with the estimated true heading.

AUTONOMOUS DRIVING CONTROL SYSTEM

Robotic Mower

In this study, we added an autonomous driving control system to a remotely controlled self-propelled robotic mower (AJK600, Sanyo Kiki Co., Ltd., Okayama, Japan) and used it for autonomous driving tests on a slope. Table 1 shows the specifications of the mower. This machine was equipped with a pair of rotary cutter blades on the bottom and was designed to cut grass from either the front or rear. This structure eliminated the need for a 180-degree U-turn during reciprocating work, which increased the efficiency compared to a mower with a front-mounted mowing unit. In addition, since there

Table 1. Specification of robotic mower used in experiment.

Item	Specifications
Engine	Honda iGX390
Maximum output	8.7 kW
Battery voltage	12 V
Rated flow rate (Hydraulic pump)	22 L min^{-1}
Rated pressure (Hydraulic pump)	13.7 MPa
Total length/Total width	1260/1160 mm
Mowing width	600 mm
Weight	200 kg
Vehicle speed	Maximum 0.77 m s^{-1}
Steering system	4-wheel skid steer

was no need for turning with large angle changes when working on slopes, the risk of the mower falling over was reduced. The machine was equipped with a gasoline engine, and the power of the engine drove two disk blades and a hydraulic pump via belts. The hydraulic oil sent from the hydraulic pump was divided into two channels, left and right, to drive the hydraulic motors on both sides of the machine. Independent solenoid directional control valves and solenoid proportional valves controlled the forward and backward motion and speed of the machine, respectively. The front and rear tires were connected by chains, resulting in a 4-wheel skid steer system. Steering was done by varying the number of revolutions of the left and right wheels or by reversing the revolutions of the left and right wheels (spin turn). The rotation of the disk blades was turned on and off by manually operating the tensioner of the drive belt with a lever. This machine was capable of mowing on a slope of up to 40°.

Overview of the Device and the Autonomous Driving Control System

Figure 4 shows the appearance of the mower equipped with the autonomous driving control system. A frame for mounting the GNSS antenna was attached to the mower. The antenna for a rover receiver was installed in front of the center of the mower, and the antenna for a base receiver was installed behind the center of the mower. The distance between the two antennas was 50 cm to fit the size of the mower, although the longer the distance was, the more accurate the heading measurement. The height of each antenna was 1.025 m above the ground. The inertial measurement unit (IMU) (3DM-GX5-45, LORD Microstrain, Cary, N.C.) was mounted on the bottom of the antenna frame. The control box was equipped with a prototype GNSS compass, a single board computer (LattePanda 4G/64GB, LattePanda, Shanghai, China) with Intel Cherry Trail Z8350 and 4 GB RAM, and a wireless module to communicate with the controller of the robot mower.

The block diagram of the autonomous driving control system is shown in figure 5. The position and heading angle of the robotic mower were processed by a single board computer and used for autonomous driving control. Ground control station (GCS) software was installed on a PC or an Android tablet to send and receive information on the robotic mower position and route via the network. The details of the GCS are described in the next section. The robot operating system (ROS) platform was used for inter-process communication between autonomous driving programs and the GNSS message parsing program.

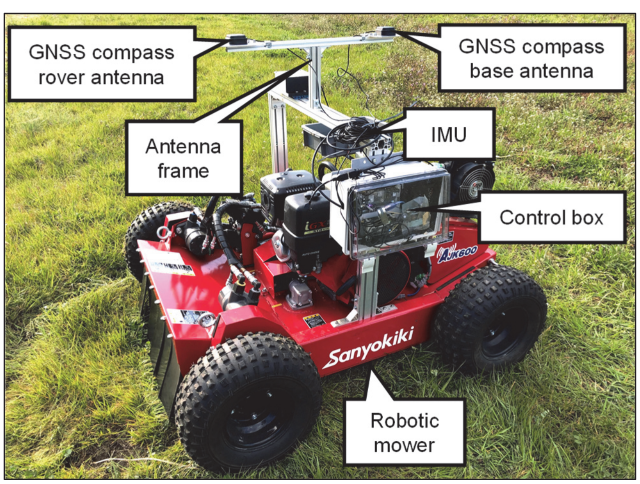

Figure 4. Overview of robotic mower equipped with autonomous driving system.

The prototype GNSS compass used an RTK function and a moving-base RTK function of the receivers to output the position and heading angle of the robotic mower. The first receiver measured the position using the RTK function and output correction data to the second receiver for the heading measurement. Radio technical commission for maritime services (RTCM) correction messages must be sent to the mobile station to use RTK positioning. To obtain the RTCM correction messages, the networked virtual reference station (VRS)-RTK service was used. Since this service required internet communication, a cellular network was used. The positioning result of RTK was set to output at 5 Hz. To achieve moving-base RTK positioning, RTCM 1077, 1087, 1230, and 4072.0 were output from the mobile reference station (4072.0 was a custom RTCM message of u-blox). The transmission of RTCM messages from the moving base station to the rover station was done by connecting the universal asynchronous receiver/transmitter (UART) ports of the receivers. Moving-base RTK positioning results were set to output at 5 Hz. The heading of the robotic mower was calculated from the relative position of the mobile station to the moving base station.

Open-source software for drones called QGroundControl (QGC) was used as GCS (Dronecode Project Inc, 2021). By communicating with the QGC via a protocol called MAVLink, an autonomous driving route can be set using a map shown in a graphical user interface (GUI) of the map (fig. 6). The program developed in this study consisted of subprograms that converted latitude and longitude, GNSS positioning status, control constants, and autonomous driving routes into MAVLink format for transmission and reception. This made it possible to use a PC or Android tablet to monitor the status of the machine, set the autonomous route, change the control constants, and instruct the system to start driving autonomously.

Tilt Correction for Driving on Slopes

Since the GNSS antenna was installed above the top of the robotic mower, when the machine tilted, the position (GNSS coordinate) of the antenna deviated from the center position of the bottom of the robotic mower, resulting in a position error. To compensate for the effects of tilt, roll, and pitch, angles measured with an IMU were used. We defined a right-handed orthogonal coordinate system (XYZ) as the world coordinate system (UTM) with the positive Z-axis oriented vertically upward. For the vehicle coordinate system, an orthogonal right-handed system (xyz) was defined with the forward direction of the vehicle as the x-axis, the left direction as the *y*-axis, and the vertical upward direction as the z-axis. A schematic drawing of the ground and vehicle coordinate systems is shown in figure 7, where the rotation angle around the x-axis was defined as the roll angle θ_r, and the rotation angle around the y-axis was defined as the pitch angle θ_p. The angle between the X-axis and the x-axis was defined as the yaw angle θ_y. Since this was a right-handed

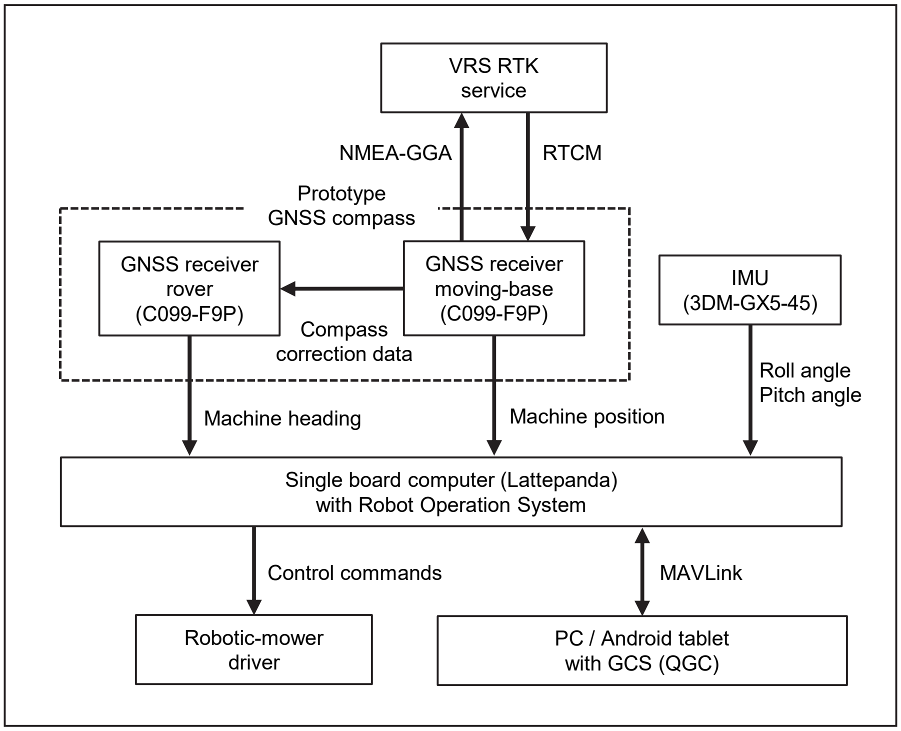

Figure 5. Schematic diagram of autonomous driving control system.

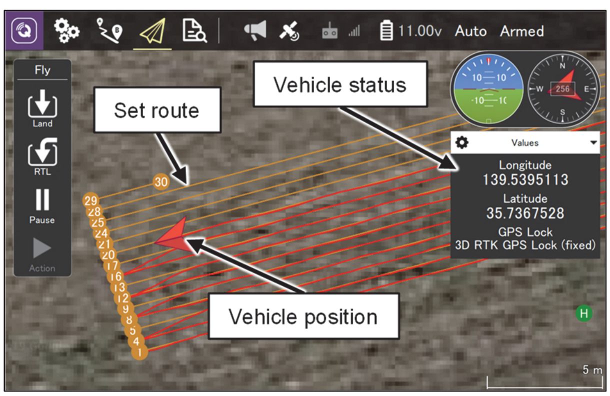

Figure 6. Graphical user interface (GUI) of GCS software QGroundControl.

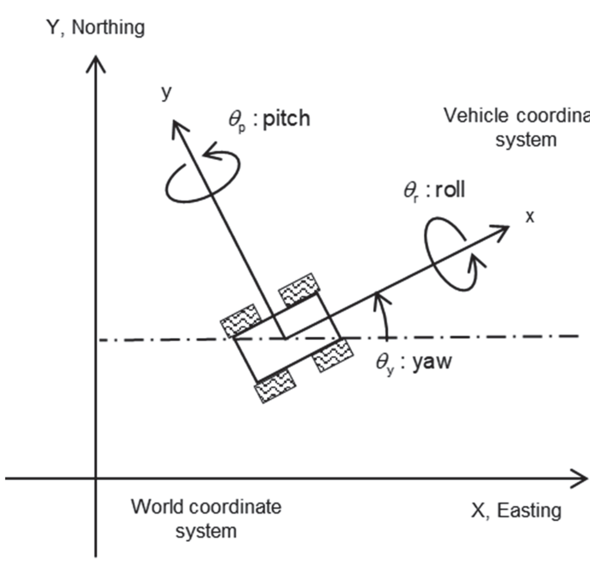

Figure 7. World coordinate system and vehicle coordinate system.

system, the positive direction of any rotation angle was counterclockwise to the rotation axis.

To correct the position error caused by tilt, it was necessary to obtain a transformation matrix to make each rotation angle of the vehicle coordinate system horizontal. This transformation matrix **R** was obtained from the following rotation matrix:

$$\mathbf{R}_{\mathrm{r}} = \begin{pmatrix} 1 & 0 & 0 \\ 0 & \cos\theta_{\mathrm{r}} & -\sin\theta_{\mathrm{r}} \\ 0 & \sin\theta_{\mathrm{r}} & \cos\theta_{\mathrm{r}} \end{pmatrix} \tag{1}$$

$$\mathbf{R}_{\mathrm{p}} = \begin{pmatrix} \cos\theta_{\mathrm{p}} & 0 & \sin\theta_{\mathrm{p}} \\ 0 & 1 & 0 \\ -\sin\theta_{\mathrm{p}} & 0 & \cos\theta_{\mathrm{p}} \end{pmatrix} \tag{2}$$

$$\mathbf{R}_{\mathrm{y}} = \begin{pmatrix} \cos\theta_{\mathrm{y}} & -\sin\theta_{\mathrm{y}} & 0 \\ \sin\theta_{\mathrm{y}} & \cos\theta_{\mathrm{y}} & 0 \\ 0 & 0 & 1 \end{pmatrix} \tag{3}$$

$$\mathbf{R} = \mathbf{R}_{\mathrm{y}} \cdot \mathbf{R}_{\mathrm{p}} \cdot \mathbf{R}_{\mathrm{r}} \tag{4}$$

where $\mathbf{R}_{\mathrm{r}}$ is the rotation matrix of the roll angle, $\mathbf{R}_{\mathrm{p}}$ is the rotation matrix of the pitch angle, and $\mathbf{R}_{\mathrm{y}}$ is the rotation matrix of the yaw angle. From the position of the GNSS antenna in the vehicle coordinate system (x_0, y_0, z_0), the tilt correction (Δx, Δy, Δz) was obtained as follows:

$$\begin{pmatrix} \Delta x \\ \Delta y \\ \Delta z \end{pmatrix} = \mathbf{R} \begin{pmatrix} -x_0 \\ -y_0 \\ -z_0 \end{pmatrix} \tag{5}$$

From (Δx, Δy, Δz) and the position of the GNSS antenna in the ground coordinate system (X_{GNSS}, Y_{GNSS}, Z_{GNSS}), the coordinates of the center of the bottom of the robotic mower in the ground coordinate system (X', Y', Z') was obtained as follows:

$$\begin{pmatrix} X' \\ Y' \\ Z' \end{pmatrix} = \begin{pmatrix} X_{\text{GNSS}} \\ Y_{\text{GNSS}} \\ Z_{\text{GNSS}} \end{pmatrix} + \begin{pmatrix} \Delta x \\ \Delta y \\ \Delta z \end{pmatrix} \tag{6}$$

The coordinates of the bottom of the robotic mower (X', Y', Z') were used to define the position of the robotic mower for the calculation of the autonomous driving control.

Algorithm for Autonomous Driving Control

Figure 8 shows an overview of the autonomous driving control. To follow the set path, a target point was set on a straight-line path, and it moved with the movement of the mower while maintaining the look-ahead distance (L_A). The heading was controlled to move toward this point. To perform this control, the relative bearing of the robotic mower (φ_r) was calculated as follows:

$$\varphi_{\text{r}} = \varphi_{\text{b}} - \varphi_{\text{h}} \tag{7}$$

where φ_b is the bearing, which is the direction to the moving target point, and φ_h is the heading of the robotic mower. This relative bearing (φ_r) was multiplied by a proportional gain (K_p) and converted into a steering value that was sent to the mower driver to control the machine, making it move toward the target point on the path. However, this control alone generated a steady error in the lateral direction of the path due to bias in the steering characteristics. In addition, if the vehicle runs on a slope, errors also occur due to slippage down the slope. To suppress these deviations, the lateral distance (d) was multiplied by the control constant (K_{cte}) and this product was added to the steering value. This steering value (S_{in}) was calculated as follows:

$$S_{\text{in}} = K_{\text{p}} \cdot \varphi_{\text{r}} + K_{\text{cte}} \cdot d \tag{8}$$

Notably, if the mower was too far away from the setting path, the value of the steering control for cross-track error became very large, causing the mower to oversteer, so a limit was set. The proportional gain (K_p) and the control constant (K_{cte}) were experimentally obtained and optimized. Based on the results of runs on a slope with different parameters in the preliminary experiments, the parameters with the lowest cross-track error and the least oscillation of the trajectory were chosen. The values of L_A, K_p and K_{cte} were 1.3, 0.2, and 1.2, respectively. The algorithm described above enabled autonomous driving along the route. In this experiment, no curved paths were set up for turns between straight paths. When the mower arrived at the end of a straight path, it switched back and was controlled to follow the next straight path.

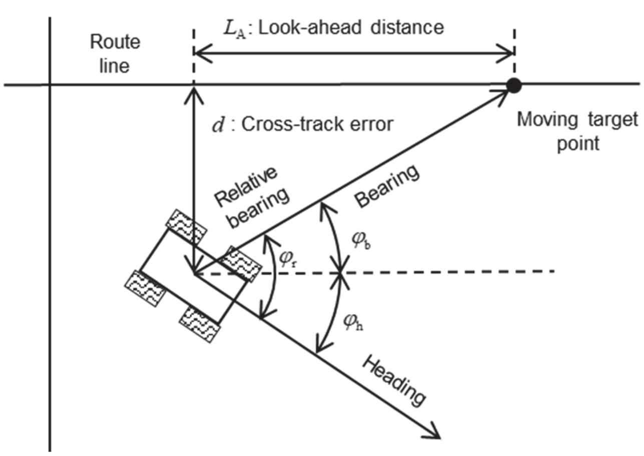

Figure 8. Diagram of autonomous control of robotic mower.

AUTONOMOUS DRIVING TEST

Setting Up the Test Site and Autonomous Driving Route

The autonomous driving test was conducted in March 2020 at Osakaike Pond in Kasaoka City, Okayama, Japan (latitude: 34.559644° N, longitude: 133.534793° E). The experimental site was the slope of the embankment of an agricultural earth dam, as shown in figure 9. The angle of the slope was approximately 25°, and there was no unevenness on the surface of the ground that could cause the robotic mower to become stuck. As a first trial to examine the ability of autonomous driving under conditions with little disturbance, the capability of the mower to drive autonomously was tested without mowing the grass. (We are planning to conduct future autonomous mowing tests under various conditions.) The working speed of the robotic mower was approximately 0.52 m s^{-1} in this experiment. The autonomous driving route was prepared using a QGC with a mode to set a rectangular area on a map and create parallel paths within a rectangle. Using this function, the distance between the routes was set to 0.4 m, the length of the routes was 40 m, and the number of routes was 11. The route was set to follow contour lines. Because two cases of driving the machine, down from the top of the slope or up from the bottom of the slope, are possible in mowing, both were tested and compared.

Evaluation Method of Autonomous Driving

The accuracy of autonomous driving was evaluated by calculating the cross-track error. The cross-track error was the deviation between the set path of 11 routes and the

Figure 9. Experimental site (Osakaike Pond).

autonomous driving trajectory, and the calculation was performed using the positioning data of an RTK-GNSS receiver.

RESULTS AND DISCUSSION

ACCURACY EVALUATION OF THE PROTOTYPE GNSS COMPASS

Heading Error under Horizontal Conditions with 0° Roll and 0° Pitch

Table 2 shows the average values and RMS error (RMSE) of the heading of the prototype GNSS compass and the commercial GPS compass in the horizontal state. The values in the table were calculated from the data measured at each heading angle. The error in the heading of the prototype GNSS compass was estimated to be 0.58° under horizontal conditions.

Heading Error for Roll and Pitch Changes

Figure 10 shows the RMSE of the heading measured by the prototype GNSS compass with different pitch and roll values. The larger the pitch and roll values were, the larger the RMSE tended to be. When these values were both less than 45°, the RMSE was within approximately 1.5°. During this evaluation test, the fixed rate of the moving-base RTK of the prototype GNSS compass was 100.0%.

The maximum slope angle at which the mower can work is 40°. When the pitch and roll values were less than 40°, the heading error of the prototype GNSS compass was within 1.5°. The heading error affects the φ_r value in equation 8. However, the cross-track error caused by the heading error was expected to be only a few centimeters for L_A=1.3 m in this study. Therefore, we concluded that the prototype GNSS compass had sufficient heading accuracy for autonomous operation of the robotic mower on slopes.

Table 2. Heading error under horizontal conditions.

	Average of heading error (°)	RMSE of the heading (°)
Commercial GPS compass	0.00	0.22
Prototype GNSS compass	0.33	0.58

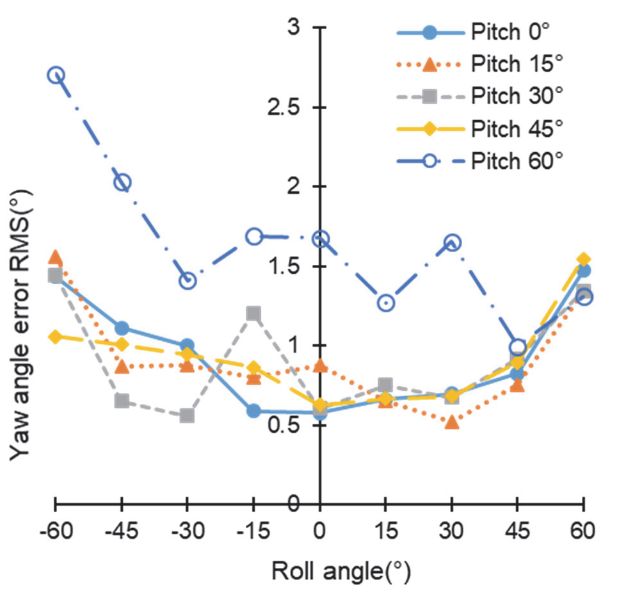

Figure 10. RMS of heading error of prototype GNSS compass.

EVALUATION OF AUTONOMOUS DRIVING

Figure 11 shows the set route and the driving trajectory when the robotic mower ran autonomously downward from the top of the slope. As shown in the graph, autonomous driving started from the upper right of the graph and ended at the lower left. For each of the 11 linear paths, the mean value and RMS of the cross-track error were calculated. The cross-track deviation immediately after the turn was large due to the path spacing. Therefore, the mean and RMS were calculated from the time when the robotic mower approached within 10 cm of the path to the end of that path. The convergence to the set path was also evaluated by calculating the time and distance traveled before the cross-track error was within 10 cm after a turn. The results of these calculations are shown in table 3 as an evaluation of the autonomous driving accuracy. The average cross-track error for the entire straight-line route was 6.7 cm, and the RMSE was 7.2 cm. The mower mostly traveled at a lower elevation than the specified trajectory because when traveling on a slope, the mower was pulled downward by gravity. However, considering that the horizontal accuracy of the RTK positioning of the GNSS receiver used in this experiment was 1.0 cm CEP, or approximately 1.2 cm in RMSE terms, and the vehicle was driving on a slope, the accuracy of the autonomous driving system was considered to be sufficient. In addition, the cross-track error converged to within 10 cm after driving an average of 48.9 cm from the starting point of the straight path (after an average of 2.4 seconds from the starting point). Figure 12 shows the graphs of the cross-track errors for the 6th, 8th, and 10th paths. According to the graphs, there were some sections where the cross-track error exceeded 10 cm even after convergence. However, in most of the sections, the cross-track error was within 10 cm, and the same tendency was observed for other linear paths not shown in the figure.

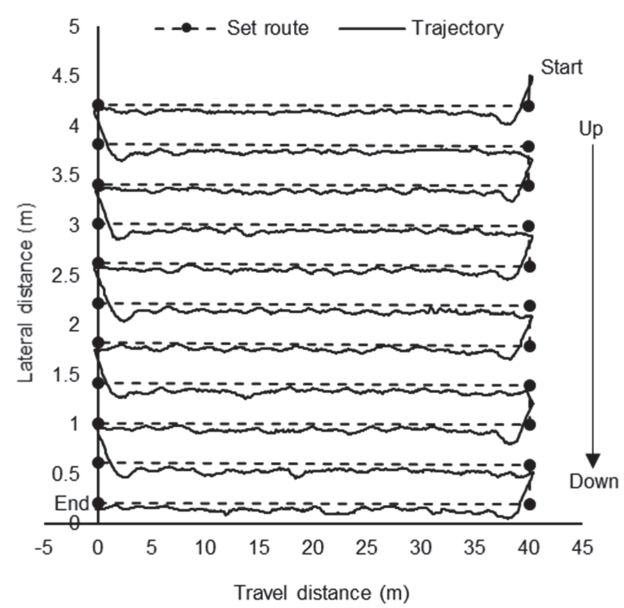

Figure 11. Trajectory of autonomous driving and reference straight line paths (driving from top of slope).

Table 3. Results of autonomous driving (driving from the top of the slope).

Path	1	2	3	4	5	6	7	8	9	10	11	Ave.
Average cross-track error (cm)	6.9	6.7	6.2	6.8	5.9	7.4	5.5	7.4	6.4	7.7	6.6	6.7
RMS cross-track error (cm)	7.4	7.2	6.7	7.2	6.4	7.9	6.0	7.9	7.1	8.2	7.4	7.2
Time to convergence within 10 cm (s)	2.4	2.4	1.8	2.4	2.2	2.4	2.4	2.4	2.0	2.8	2.6	2.3
Distance traveled until convergence within 10 cm (cm)	45.1	49.5	28.6	59.1	45.3	61.6	58.9	46.9	27.6	70.9	44.3	48.9
Maximum cross-track error after convergence to within 10 cm (cm)	18.6	10.6	15.8	15.7	13.8	17.9	13.9	15.2	19.1	14.8	14.5	15.4

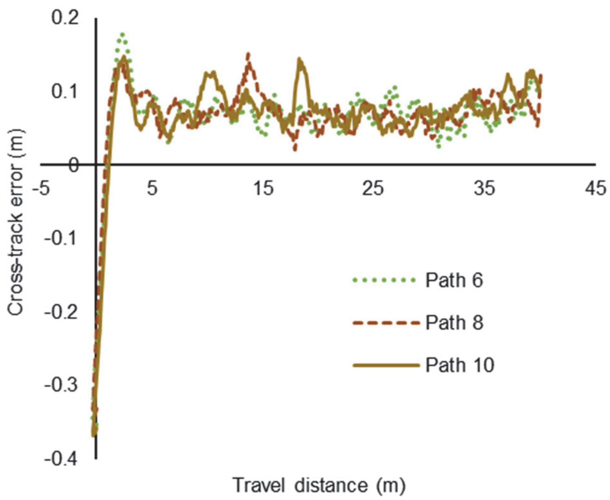

Figure 12. Cross-track error in autonomous driving (driving from top of slope).

Figure 13 shows the changes in heading during autonomous driving for three typical paths. The measured heading was continuous, and there was no major breakdown. The percentage of fix solutions obtained for all epochs was 100%. This figure also shows that the mower was traveling with its heading slightly upward.

Figure 14 shows a graph of the set route and the running trajectory when the robot ran autonomously upward from the bottom of the slope. As shown in the graph, autonomous driving started at the lower right of the graph and ended at the upper left. As with driving from top to bottom, the mower generally traveled at a lower elevation than the prescribed trajectory. Near the beginning of the straight path, the robot mower went down the slope to deviate from the course and then went up again to return to the course. The reason for this move is discussed below. Once the robotic mower began to travel along the course, it did not deviate notably from the course. The results of the autonomous driving accuracy are shown in table 4. For the cross-track error, the average value for the entire straight path was -6.3 cm, and the RMSE value was 6.6 cm. The cross-track errors converged to within 10 cm after an average of 510.2 cm and 12.3 seconds from the start of the straight path, indicating that it took longer to converge than when traveling downward from the top of the slope. Figure 15 shows the graphs of the cross-track errors for 5th, 7th, and 9th paths. According to the graphs, there were sections where the cross-track error exceeded 10 cm even after convergence. However, in most of the sections, the cross-track error was within 10 cm, and the same tendency was observed for other straight paths not shown on the graph.

The reason that the robotic mower moved away from the target path once during each test near the starting point of every path is discussed here. Figure 16 shows a plot of the trajectory and heading of the robotic mower near the end of the first straight path. The directions of the arrows indicate the heading of the robotic mower obtained from the prototype GNSS compass. According to the graph, the heading of the mower was always in the direction of climbing up the slope because when the robotic mower was running, gravity caused it to slide down the slope, and it was necessary to steer the mower up the slope to follow the path. At the end of the path, the heading still faced up the slope (red dotted

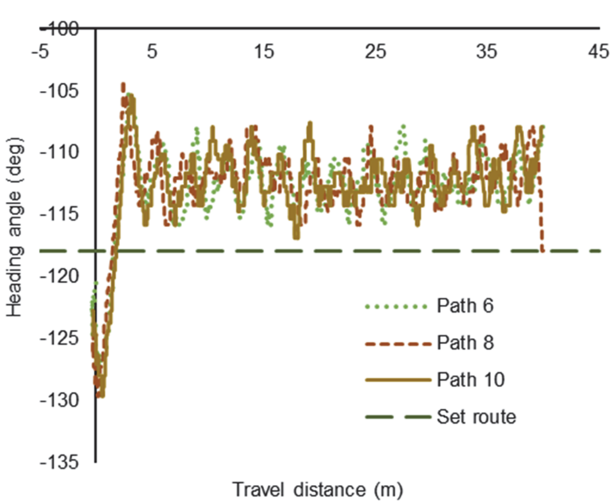

Figure 13. Heading during autonomous driving (driving from top of slope).

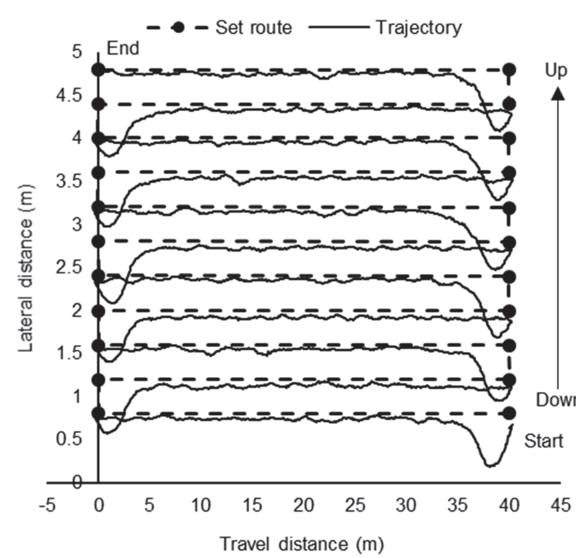

Figure 14. Trajectories of autonomous driving and reference straight line paths (driving upward from bottom of slope).

Table 4. Results of autonomous driving (driving upward from the bottom of the slope).

Path	1	2	3	4	5	6	7	8	9	10	11	Ave.
Average of cross-track error (cm)	-6.1	-8.0	-5.3	-8.3	-4.9	-7.7	-5.4	-6.8	-4.6	-6.9	-5.0	-6.3
RMS of cross-track error (cm)	6.4	8.3	5.8	8.4	5.3	7.8	5.8	7.1	4.9	7.1	5.3	6.6
Time to convergence within 10 cm (s)	13.2	12.4	10.6	10.4	11.4	12.8	14.8	12.4	12.6	13.4	11.6	12.3
Distance traveled until convergence within 10 cm (cm)	530.7	510.7	419.5	426.8	471.4	548.5	638.9	522.3	504.6	575.1	463.6	510.2
Maximum cross-track error after convergence to within 10 cm(cm)	10.7	13.2	12.1	11.6	10.5	11.6	11.3	14.5	9.5	10.6	10.4	11.5

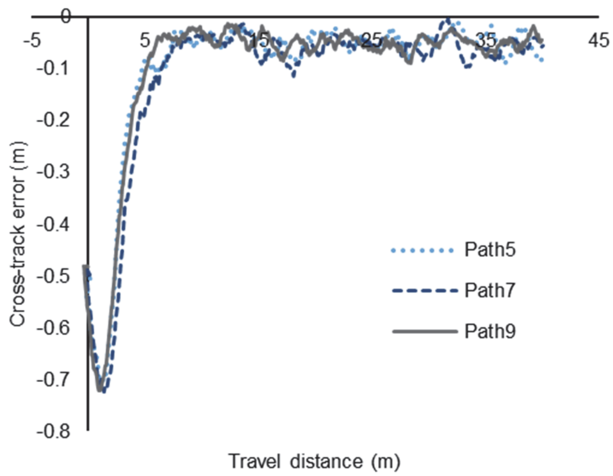

Figure 15. Cross-track error in autonomous driving (driving upward from bottom of slope).

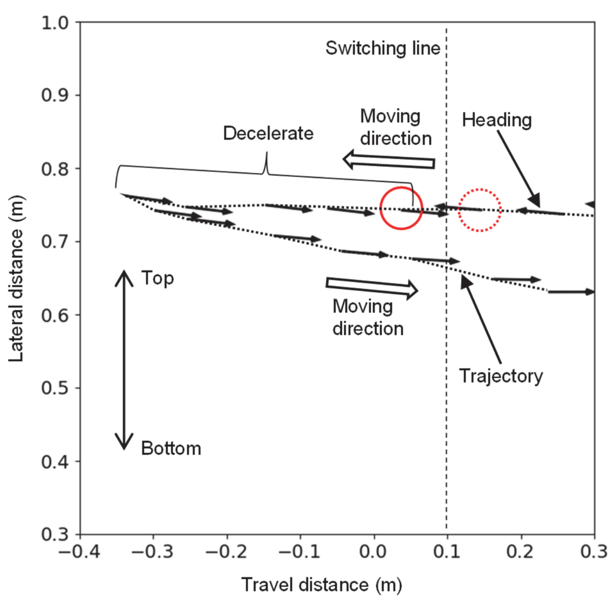

Figure 16. Trajectory and heading of robotic mower at edge of path moving from bottom to top of slope.

circle). When the robotic mower detected that it had crossed the switching line 10 cm before the waypoint, the front and back of the mower were virtually switched in the software. Because the actual orientation of the mower did not change, its heading pointed down the slope from this control period. As a result, the mower moved once toward the bottom of the slope. A pivot turn would be an effective way to eliminate this unnecessary movement and move the mower to the next path more quickly.

During the slope test, the speed of the mower was approximately 0.52 m s^{-1} and an overshoot of approximately 30 cm was observed at the waypoint because the mower did not decelerate until it passed the switching lines. To reduce the overshoot, additional speed control is necessary.

Conclusions

To realize an autonomous robotic mower capable of mowing grass on slopes, we developed an autonomous driving control system using a low-cost dual-frequency GNSS compass (prototype GNSS compass), a low-cost dual-frequency RTK-GNSS, and an IMU. To evaluate the heading accuracy of the prototype GNSS compass, an evaluation system was developed; it used the heading of a commercial GPS compass as a reference. The RMS of the heading error of the prototype GNSS compass was 0.58° under horizontal conditions, which was sufficiently accurate for the autonomous driving control of the mower. In addition, the tilting test of the prototype GNSS compass showed that the heading error was within 1.5° RMS when the roll and pitch values were less than 45°. In the automatic driving experiment, the prototype GNSS compass continuously measured the angle of the vehicle without any breakdown. In conclusion, the prototype GNSS compass was practical with little loss of heading accuracy, even when on slopes.

In the test of autonomous driving downward along contour lines from the top of a slope, the RMSE of the cross-track of the set path was 7.2 cm. In the test of autonomous driving upward along the contour lines from the bottom of the slope, the RMSE of the cross-track against the set path was 6.6 cm.

In both tests, the mower traveled slightly lower down the slope than the set path, corresponding to a steady-state deviation in control engineering. This steady-state deviation could be reduced by adding a term for the time integration of the lateral deviation to the steering value in equation 8.

At the beginning of every path, the robotic mower moved downward once. Future improvements were recommended, such as having the robot make a pivot turn near the start of a path, to suppress the deviation.

The mower used in this study had a cutting width of 60 cm and a spacing of 40 cm between straight paths, so there was no uncut grass as long as the cross-track error was within 10 cm. The cross-track error was within 10 cm in most sections of each run. Sufficient accuracy was obtained for autonomously mowing the grass on the slope. The results confirmed that the mower with the developed GNSS compass could be driven stably and autonomously even on an inclined surface of approximately 25°, which was the condition in this study.

In conclusion, the results of this study demonstrated the feasibility of adding an autonomous driving function to a self-propelled machine at low cost and applying it to driving on slopes.

ACKNOWLEDGMENTS

This research was supported by grants from the Project of the Bio-oriented Technology Research Advancement Institution, NARO (the special scheme project on advanced research and development for next-generation technology).

REFERENCES

Bell, T. (2000). Automatic tractor guidance using carrier-phase differential GPS. *Comput. Electron. Agric., 25*(1), 53-66. https://doi.org/10.1016/S0168-1699(99)00055-1

Bochtis, D. D., Vougioukas, S. G., & Griepentrog, H. W. (2009). A mission planner for an autonomous tractor. *Trans. ASABE, 52*(5), 1429-1440. https://doi.org/10.13031/2013.29123

Carballido del Rey, J., Pérez-Ruiz, M., Emmi, L., & Agüera Vega, J. (2014). Comparison of positional accuracy between RTK and RTX GNSS based on the autonomous agricultural vehicles under field conditions. *Appl. Eng. Agric., 30*(3), 361-366. https://doi.org/10.13031/aea.30.10342

Dronecode Project Inc. (2021). QGroundControl. Retrieved from http://qgroundcontrol.com/

Hemisphere Inc. (2010). VS101 and VS111 GPS compass professional heading and positioning receiver. Retrieved from http://www.canalgeomatics.com/product_files/vs101-gps-compass_375.pdf

Igarashi, S., Kaizu, Y., Tsutsumi, T., & Imou, K. (2020). Development of an autonomous driving control system for a robotic mower using a low-cost single-frequency GNSS compass. *J. Japanese Soc. Agric. Mach. Food Eng., 82*(6), 609-616.

Iida, M., Uchida, R., Zhu, H., Suguri, M., Kurita, H., & Masuda, R. (2013). Path-following control of a head-feeding combine robot. *Eng. Agric. Environ. Food, 6*(2), 61-67. https://doi.org/10.11165/eaef.6.61

Kaizu, Y., Tokuda, H., Yamada, H., & Imou, K. (2015). Development of an electric-powered, unmanned airboat for lake environment monitoring. *J. Japanese Soc. Agric. Mach. Food Eng., 77*(6), 477-484. https://doi.org/10.11357/jsamfe.77.6_477

Kaizu, Y., Tsutsumi, T., Igarashi, S., & Imou, K. (2018). Development of an autonomous driving control system for a robot mower using a low-cost single-frequency GNSS and a low-cost IMU. *J. Japanese Soc. Agric. Mach. Food Eng., 80*(5), 271-279.

Lindgren, D. R., Hague, T., Smith, P. J., & Marchant, J. A. (2002). Relating torque and slip in an odometric model for an autonomous agricultural vehicle. *Autonomous Robots, 13*(1), 73-86. https://doi.org/10.1023/A:1015682206018

Mashadi, B., & Nasrolahi, H. (2009). Automatic control of a modified tractor to work on steep side slopes. *J. Terramech., 46*(6), 299-311. https://doi.org/10.1016/j.jterra.2009.08.006

Mochizuki, Y., Iida, M., Kurita, H., Cho, W., & Suguri, M. (2015). Corner harvesting method for a head-feeding combine robot. *J. Japanese Soc. Agric. Mach. Food Eng., 77*(6), 464-469. https://doi.org/10.11357/jsamfe.77.6_464

Mousazadeh, H. (2013). A technical review on navigation systems of agricultural autonomous off-road vehicles. *J. Terramech., 50*(3), 211-232. https://doi.org/10.1016/j.jterra.2013.03.004

Qureshi, U., & Golnaraghi, F. (2017). An algorithm for the in-field calibration of a MEMS IMU. *IEEE Sens. J., 17*(22), 7479-7486. https://doi.org/10.1109/JSEN.2017.2751572

Rains, G. C., Faircloth, A. G., Thai, C., & Raper, R. L. (2014). Evaluation of a simple pure pursuit path-following algorithm for an autonomous, articulated-steer vehicle. *Appl. Eng. Agric., 30*(3), 367-374. https://doi.org/10.13031/aea.30.10347

Roshanianfard, A., Noguchi, N., Okamoto, H., & Ishii, K. (2020). A review of autonomous agricultural vehicles (The experience of Hokkaido University). *J. Terramech., 91*, 155-183. https://doi.org/10.1016/j.jterra.2020.06.006

Shen, H.-M., Lian, C., Wu, X.-W., Bian, F., Yu, P., & Yang, G. (2021). Full-pose estimation using inertial and magnetic sensor fusion in structurized magnetic field for hand motion tracking. *Meas.: J. Int. Meas. Confed., 170*, 108697. https://doi.org/10.1016/j.measurement.2020.108697

Tamaki, K., Segawa, T., Shibuya, Y., & Iijima, W. (2006). Development of an autonomous running technique for wide fertilizer spreading on sloping grasslands (Part 2) : Improved speed control. *J. Japanese Soc. Agric. Mach. Food Eng., 68*(3), 65-71. https://doi.org/10.11357/jsam1937.68.3_65

u-blox, AG. (2020). ZED-F9P u-blox F9 high precision GNSS module Data sheet.

Wang, X., Thorp, K. R., White, J. W., French, A. N., & Poland, J. A. (2016). Approaches for geospatial processing of field-based high-throughput plant phenomics data from ground vehicle platforms. *Trans. ASABE, 59*(5), 1053-1067. https://doi.org/10.13031/trans.59.11502